The Local and Nonlocal Response of Conception Bay to Wind Forcing

BRAD DE YOUNG, TIMM OTTERSON, AND RICHARD J. GREATBATCH

Department of Physics, Memorial University of Newfoundland, St. John's, Newfoundland, Canada

(Manuscript received 20 April 1992, in final form 5 January 1993)

ABSTRACT

In this paper the response of Conception Bay to wind forcing is discussed. Current meter and thermistor chain observations are analyzed and compared with output from a reduced-gravity numerical model. The model incorporates realistic coastal geometry and is driven by wind stress calculated from observed winds.

Moorings were deployed in the bay during 1989 and 1990. In 1990 the moorings were placed within the coastal waveguide around the head of the bay and show that southwesterly winds generate an upwelling event on the western side that moves around the head of the bay and is suggestive of Kelvin wave propagation. Data analysis shows that the thermocline response is strongly coherent between each mooring at periods of 2–10 days, and winds measured at a nearby station are found to be strongly coherent with the observed temperature fluctuations.

Two versions of the reduced-gravity model are applied—one models Conception Bay alone and ignores "upstream" influences and another includes neighboring Trinity Bay, located to the northwest and "upstream" in the sense of Kelvin wave propagation. The local model does reasonably well at reproducing the observed movement of the thermocline but underestimates its amplitude. The nonlocal model, which includes the neighboring bay, does much better at simulating the observations, including the amplitude of the response, and also the upper-layer currents. The comparisons clearly show the importance of nonlocal effects.

1. Introduction

In this paper, we investigate the response of Conception Bay, Newfoundland, to wind forcing (see Fig. 1). The work forms part of a project to understand primary production in a cold ocean system, the Cold Ocean Productivity Experiment (COPE), that is concerned with temperature variations at seasonal and synoptic periods. Here we concentrate on the synoptic band, looking at the response of the bay to wind forcing. Data from the bay show large daily vertical movements of the thermocline of up to 10–20 m. We shall investigate these events with periods of 2–10 days using a reduced-gravity numerical model driven by wind stress calculated from observed winds. The model is capable of simulating upwelling events in the bay and enables us to assess the importance of nonlocal effects due to coastal-trapped wave propagation from neighboring Trinity Bay.

In using a reduced-gravity model, we are implicitly assuming that density stratification is playing a more important role in determining the coastal-trapped wave response of the bay than the underlying bottom topography. The important parameter that measures this is the stratification parameter S defined by

$$S = \frac{N_0^2 H^2}{f^2 L^2},$$

where N_0 and L are representative scales for the buoyancy frequency and the cross-shore topography in the bay, H is the maximum depth, and f is the Coriolis parameter. Huthnance (1978) has shown that in the limit $S \ll 1$ (corresponding to weak stratification), coastal-trapped waves are more like barotropic shelf waves, whereas for $S \gg 1$ (corresponding to strong stratification), they are more like baroclinic coastal Kelvin waves. Wang and Mooers (1976) showed that in the intermediate range of $S \sim 1$, waves of a hybrid character occur. These authors also showed that if a coastal wall can be assumed, waves with the characteristics of baroclinic coastal Kelvin waves exist, whatever the stratification. In section 3, where we discuss the model, we shall argue that for the time of year we consider in Conception Bay, S has a value of about 10. As such, density stratification can be expected to play a strong role. We are helped in this by the steep sides of the bay (see Fig. 1), which limit the size of the length scale L.

Evidence for the existence of baroclinic Kelvin wave propagation is discussed in Gill (1982, section 10.13). Examples are given from along the Pacific coast of North America and in the Great Lakes (see also Clarke 1977). In most of the cases presented, the topography slopes steeply from the shore with a narrow shelf region, if a shelf is present at all, indicating the dominance of

Corresponding author address: Dr. Brad de Young, Department of Physics, Memorial University of Newfoundland, St. John's, Newfoundland, Canada, A1B 3X7.

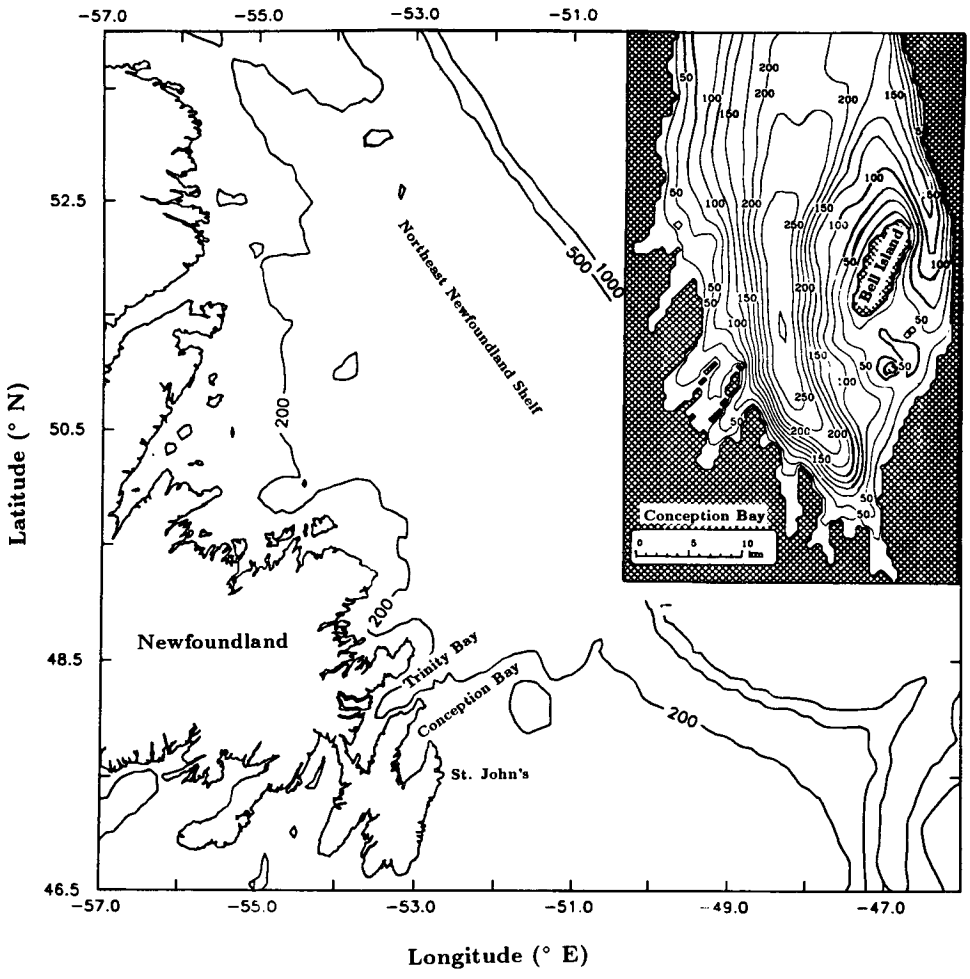

FIG. 1. Northeast coast of Newfoundland. Depth contours are in meters. Conception Bay is shown in the insert and is located on the southeastern end of the island about 30 km west of St. John's, the capital city. Bottom contours are shown in meters.

density stratification and a large value for S. In section 2, we will present data collected from moorings deployed in Conception Bay that indicate upwelling events driven by Ekman transport that is offshore from the west coast of the bay. These upwelling events propagate around the bay with a phase speed characteristic of Kelvin waves.

Since the dominant events in the bay occur on a time scale of 2–10 days, our interest is restricted to subinertial time scales. Gill and Clarke (1974) showed that in this case (and provided the alongshore length scale is large compared to the cross-shore scale) the response of the coastal waveguide to wind forcing can be reduced to solving the forced, one-dimensional wave equation. This is true not only for baroclinic coastal Kelvin waves and barotropic continental shelf waves, but also for quite general, coastal-trapped waves, as pointed out by Clarke (1977). As such, our reduced-gravity model is suitable for studying the response of Conception Bay to wind forcing, even if the waves that propagate along the coast are really hybrid waves and not strict baroclinic Kelvin waves. This is because, as noted by Gill and Clarke (1974), the shallow-water equations solved by our model reduce, under the same assumptions, to the forced one-dimensional wave equation. The important thing is to choose the correct wave speed at which the wave propagates. For our model, this wave speed is chosen to be the propagation speed indicated by the data to be discussed in section 2. It follows that even if the limit $S \gg 1$ is not strictly appropriate in our case, the model we use is still suitable for studying the response of the bay to wind (although the interpretation becomes less straightforward).

Of greater concern is the irregular nature of the bottom topography along the Newfoundland coast; in other words, wave scattering that will result from the spatial variation of S. For example, Killworth (1978, 1989a,b) has discussed the scattering of coastal Kelvin

waves by irregular bottom topography. He found that the scattering is most severe when the isopycnals intersect the topography. In Conception Bay, this happens around the shallow region in the southeast of the bay, near Bell Island (see Fig. 1). As we shall see, it is precisely in this region that the comparison between our model and the data is least satisfactory. Apart from this, the model does quite a good job of explaining movements of the thermocline in Conception Bay, at least near the coast and in the synoptic frequency band. It turns out to be important to include neighboring Trinity Bay in the model domain, indicating the importance of coastal-trapped wave propagating from Trinity Bay into Conception Bay. Proehl and Rattray (1984) showed that internal Kelvin waves generated by the wind on the shelf can propagate into an open embayment such as the Strait of Juan de Fuca. Presumably, scattering of coastal-trapped waves ultimately places a limit on how far downstream influences are felt. There is already evidence for Kelvin wave propagation around Trinity Bay, presented by Yao (1986), who used a simplified two-layer model to describe the response of Trinity Bay to wind forcing and suggested that there is coherence around the bay, from one side to the other.

Related work suggests that the relative importance of local to nonlocal forcing can vary considerably from one system to another. For example, in the fjords and inlets considered by Farmer and Osborn (1976) and Svendsen and Thompson (1978), direct wind forcing was shown to dominate at periods under 3 days while at longer periods, up to 10–20 days, nonlocal forcing may have played a role. Even at low frequencies, however, local effects can dominate, as was shown by Wang (1979) in a study of Chesapeake Bay where the response was found to be dominated by local forcing at periods up to 7 days. The results in fjords, while of interest, may not carry over to coastal embayments since rotation is unlikely to be important in fjords where the width is narrow relative to the internal Rossby radius and cross-channel velocities are weak (Klinck et al. 1981). In coastal embayments, such as the one studied here, these assumptions do not hold and rotation can be expected to play a major role.

In applying a reduced-gravity numerical model to the Conception Bay/Trinity Bay system, we are able to separate out the importance of local wind forcing over Conception Bay from the upstream influence of neighboring Trinity Bay. The model makes use of the open boundary formulation devised by Greatbatch and Otterson (1991). Similar work using a reduced-gravity model applied to the west coast of North America has been described by Pares-Sierra and O'Brien (1989) and Johnson and O'Brien (1990a,b). These latter authors note the importance of the nonlocal, equatorially forced response. The work of the O'Brien group has shown considerable success using a reduced-gravity model to simulate sea level variability in coastal and equatorial waveguides and was strong encouragement for us to apply a similar model in the Newfoundland coastal environment.

Another stimulus for our work came from review of studies attempting to correlate biological variables with the wind-forced response. Several investigators working in Conception Bay have attempted to relate wind forcing to the thermocline response, often using local wind data as a proxy variable for the thermocline signal. Frank and Leggett (1981, 1982) showed that northeasterly winds were associated with the appearance of warm surface water near the shore, thereby triggering the release of capelin larvae (*Mallotus villosus*). The warm surface water was observed to contain increased food and a reduced number of predators, thus providing favorable conditions for the emerging larvae. These studies were used to relate atmospheric and oceanic conditions to recruitment variability of capelin (Leggett et al. 1984). Taggart and Leggett (1987) further developed this model and argued that the onshore wind can be used as a measure of interannual variability of water mass exchange. In all of these studies local winds were used, either observed in the bay or at a station nearby. Clearly, a proper testing of such indices is necessary to understand the apparent link between the wind and the biology. The importance of remote forcing from Trinity Bay, which we shall demonstrate, casts doubt on the validity of an index that uses only local wind as a measure of local thermocline variability.

The outline of this paper is as follows. In the next section we describe the data collected in Conception Bay and interpret the observations. The reduced-gravity model is described in section 3, and comparisons between the model and the data are presented in section 4. A summary and discussion of the results is given in section 5.

2. Data

Conception Bay is a long (70–100 km) and narrow (~20–30 km at the mouth) bay on the east coast of the island of Newfoundland (see Fig. 1). The bay is wide with respect to the internal Rossby radius (~1–10 km) but narrow relative to the external Rossby radius (~500 km). There is a sill at about 150-m depth at the mouth, which restricts access and closes off isobaths in the bay. The maximum depth in the bay is about 300 m in the central basin. Figure 1 shows that the bottom slope is quite steep near the shore; indeed, cliffs up to 250 m surround most of the bay. The southeast region of the bay is, however, relatively shallow and flat. Note that there are three islands of varying sizes located on the southeast side of the bay.

Conception Bay was studied as part of the COPE project from 1986 to 1990. Here, we shall present data primarily from the 1990 field season. Moorings were deployed around the head of the bay from late April

to mid-July 1990 at the locations marked H1–H6 in Fig. 2. CTD data were also collected during three cruises in April, May, and June at the locations marked with a star in Fig. 2. Data from one mooring in 1989, placed on the northwest side of the bay near the mouth and marked M1 in Fig. 2, shall also be discussed. The mooring data from 1989 cover the period from mid-April to mid-October.

The water mass characteristics inside the bay are determined primarily by conditions on the Newfoundland Shelf (Petrie et al. 1991), which has direct access to the bay. Freshwater runoff from the land is relatively unimportant, and even though there is strong vertical convection in the winter, there is very little sea ice formed locally (deYoung and Sanderson 1992). Sea-ice, however, is often present in the bay in low concentrations from March to late April, advected from the north by the inshore branch of the Labrador Current (Petrie and Anderson 1983). When this sea ice becomes landfast, there will obviously be a large effect on the wind-forced response, since the wind stress cannot act on the fluid underneath the ice. The structure of the wintertime response may also differ from the summer because of the weak stratification at that time of year. Landfast ice was not present in the bay for any of the data to be discussed here.

The best available wind data for this area is from St. John's airport, located about 30 km east of the bay. These data from St. John's provide the most reliable record for the region and show good agreement with limited data collected at the head of Conception Bay in 1988 and 1989. The wind velocity data at the St. John's airport are converted into wind stress following Large and Pond (1981). Velocity is scaled by 1.25 to account for reduced velocity associated with using land-based measurements (Smith and MacPherson 1987). Wind stress is assumed to be uniform over the bay and in the same direction as at St. John's. In reality, the wind field over the bay will not be uniform as a result of topographic variations along the shore and differences in the surface roughness between land and ocean. The effect of these phenomena cannot be accurately

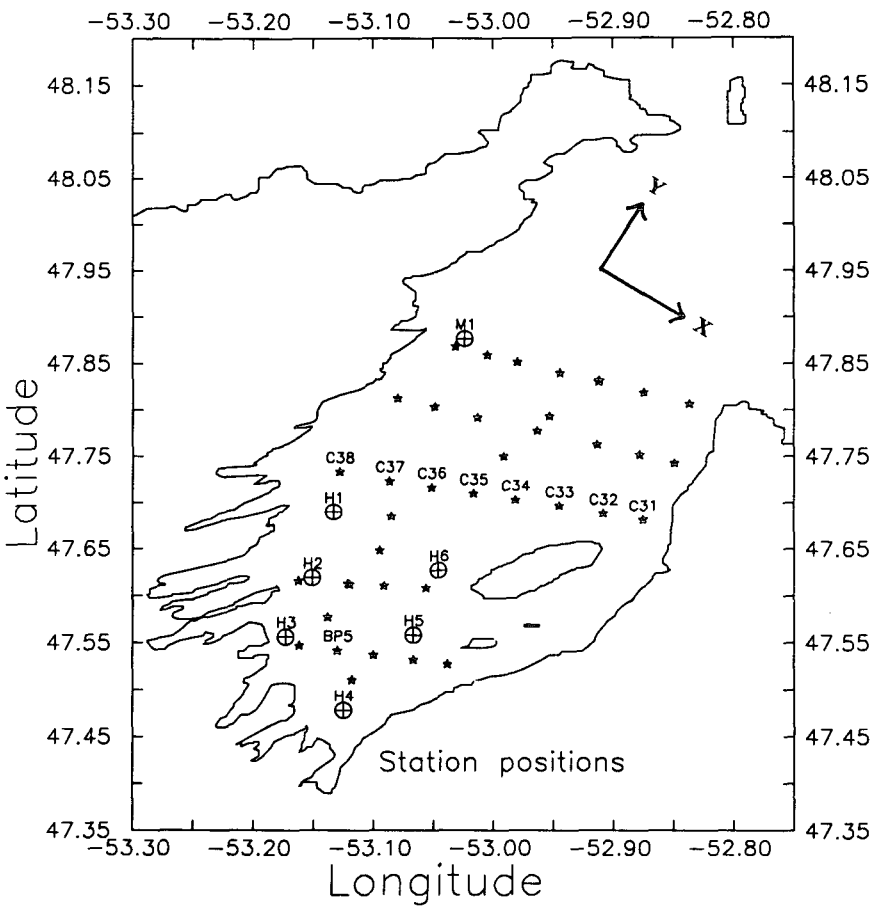

FIG. 2. CTD stations (stars) and mooring positions in Conception Bay. The moorings around the head of the bay (April–July 1990) are marked H1–H6. The mooring deployed near the mouth (April–October 1989) is marked M1. The axis near the mouth indicates the orientation of the bay coordinates referred to in the text.

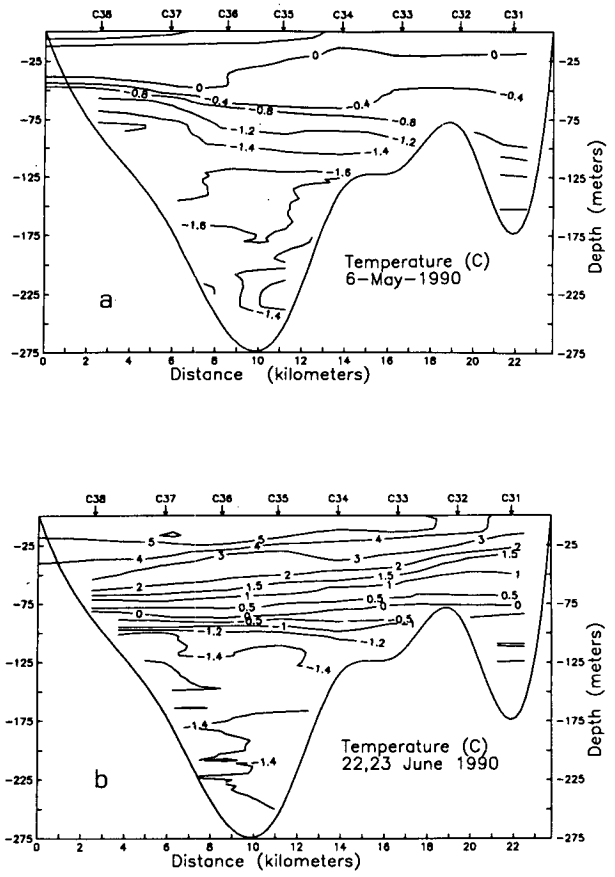

FIG. 3. Across-bay temperature field (a) for 6 May and (b) for 22–23 June 1990 calculated from CTD casts along the C3 line shown in Fig. 2. The contour interval is 0.4°C in (a) and 1°C in (b).

included, and in the absence of any data, are left out. We do not believe neglecting orographic effects to be a serious drawback because the most important wind direction for forcing the bay is along its axis, either from the southwest or the northeast, and is aligned with the coastal topography.

Figure 3 shows the temperature at stations along the C3 line (see Fig. 2) for 6 May and 22–23 June 1990. The figure shows the across-bay temperature fields, over a distance of about 23 km across the central basin of the bay. By midwinter, the entire water column is nearly homogeneous in the vertical, though there is always a weak pycnocline usually somewhere between 100 and 150 m. By late winter there is almost no vertical temperature gradient and surface water is typically $\sim -1°$ to 0°C (as in Fig. 3a) until late April or early May after the disappearance of the sea ice. Bottom water temperatures show some variability but are generally below 0°C throughout the year. By the end of June, a broad thermocline at a depth between about 25 and 100 m has developed (Fig. 3b) with surface water temperatures of 5°–7°C. By midsummer surface temperatures can reach 18°–20°C. Vertical profiles of density at BP 5 (see Fig. 2) for two times during 1990 are shown in Fig. 4. The σ_t profiles show the development of the pycnocline over the two-month period. As Fig. 4 shows, the pycnocline varies from being quite sharp as in the May profile to quite diffuse as in June.

Current and temperature data were collected from moorings deployed in late April and recovered in late July 1990 (see Fig. 2 for mooring locations). Subsurface moorings were deployed consisting of two current meters, one at ~25 m at all six moorings and another at ~100 m at moorings 2–6. Thermistor chains with 11 thermistors were placed between the two current meters at moorings 2–6, providing a vertical resolution of ~5 m in the top 50 m and ~10 m over depths 50–100 m. Moorings 1–4 were located around the head of the bay within the coastal waveguide, never more than 3–4 km from the coast. Moorings 5 and 6 were placed on the same isobaths as the first four but on the eastern side of the bay. Station separation was 8–9 km, a distance that was chosen in an effort to ensure coherence between the moorings. All of the instruments were recovered though not all of them worked properly; data recovery was about 93%. Aanderaa RCM7 current meters were used at 25 m on moorings 1 and 3, while InterOcean S4 current meters were used at 25 m on moorings 2, 4, 5, and 6. All of the bottom current meters were Aanderaas, either RCM5 or RCM7 (vector-averaging meters) instruments. All of the Aanderaa current meters were equipped with paddle-wheel rotors. The sampling interval was 15 minutes for the Aanderaa RCM5 and RCM7 and 30 minutes for the S4 meters and Aanderaa thermistor chains. Similar techniques were employed during the 1989 field season (mooring M1) for which a longer time series of data (April–October) was obtained.

All current meter, temperature, and wind data to be presented have been low-pass filtered to remove the

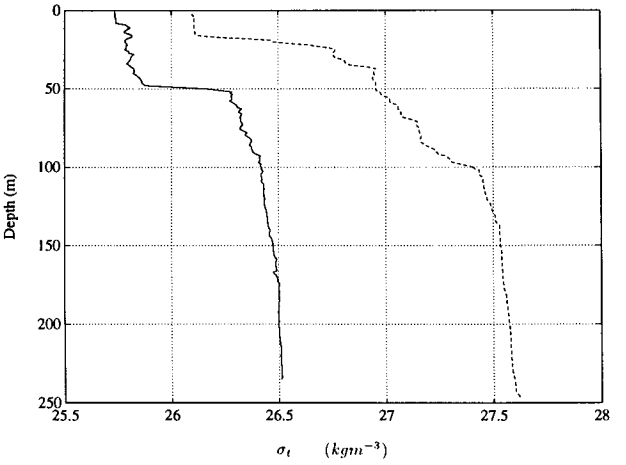

FIG. 4. Vertical profile of σ_t at station BP 5 for two periods in 1990 (a) day 148 (26 May) (b) day 173 (22 June). For easier comparison, the latter profile is offset by adding 1 kg m^{-3}.

energy with period less than 32 h. The filter was run both forward and backward to remove the effects of phase distortion. The filtering is done because we are only interested in the subinertial frequency response. The high-frequency (>2 cpd) and tidal energy comprise only a small part of the total energy in Conception Bay where typical tidal constituent velocities are 1–2 cm s^{-1} (deYoung and Sanderson 1992), thus we are focusing on the dominant signal in the record.

Figure 5 shows the temperature measured by the current meters at depth ~25 m at all six moorings over the entire period of deployment in 1990. Temperature at a fixed depth provides a way of measuring vertical motion of the thermocline. Since the water column is vertically stratified, upward movement of the thermocline brings cooler water up from below resulting in a drop in temperature at a fixed depth, while downward movement results in an increase in temperature. At early times (i.e., before day 170, 19 June 1990, close to the time of the temperature data shown in Fig. 3), stratification in Conception Bay is weak, and variations in temperature at 25 m are small. Throughout the time series, the amplitude of the temperature signal increases as the bay becomes more stratified. After day 170, all six moorings reveal similar signals although variations at moorings 5 and 6 still are comparatively weak before day 180.

Figure 6 shows a plot of temperature versus depth and time at mooring 4 as well as wind stress for the same period. The coordinate system (shown in Fig. 2) is referred to as bay coordinates, with positive y pointing out the bay and positive x pointing across the bay toward the St. John's side, the southeast side of the bay. The coordinate transformation is made by rotating 30° clockwise from true North. Comparing vertical movement of the thermocline with wind stress in the y direction, we see that at days 148, 163, 175, 183, and 190 the onset of positive wind stress corresponds to upward movement of the thermocline. Ekman transport generated by a wind blowing out the bay (i.e., $+\tau_y$) will cause upwelling along the western shore and downwelling along the eastern shore. These displacements of the pycnocline will generate waves that will propagate around the bay with the coast on their right. In Conception Bay for this time of the year, the baroclinic Kelvin wave speed is ~0.6 m s^{-1}, and the baroclinic Rossby radius of deformation, c/f, is ~6 km. Thus, for a steady wind blowing out the bay, a Kelvin wave will transmit an upwelling signal around the head in ~1 day causing a lifting of the thermocline around the head and, thus, a decrease in temperature measured at a fixed depth. When the wind relaxes, the Kelvin wave propagation will restore the bay to its undisturbed state, unless there is nonlocal forcing.

The vertical position of the thermocline can be determined using the thermistor chain data. Since the thermistor chain measures temperature at roughly 5-m depth increments within the thermocline, the vertical position of an individual isotherm can be determined fairly accurately. The depth of a specified isotherm is found by starting at the bottom of the thermistor chain and searching up the column until a depth with the

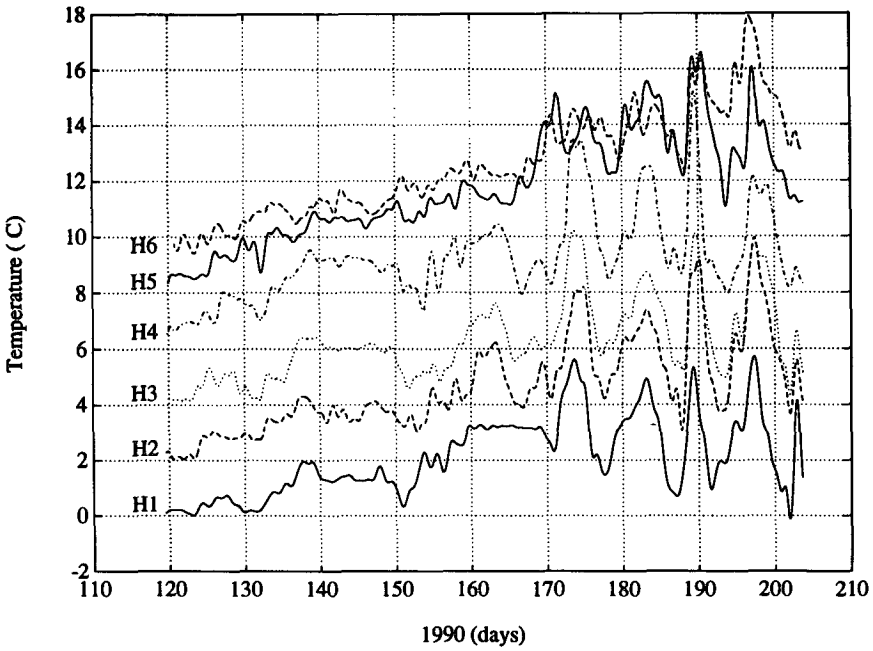

FIG. 5. Temperatures (in °C) at ~25 m at the six moorings for 1990. For easier comparison, 2°C has been added to the temperature at H2, 4°C added to the temperature at H3, and so on.

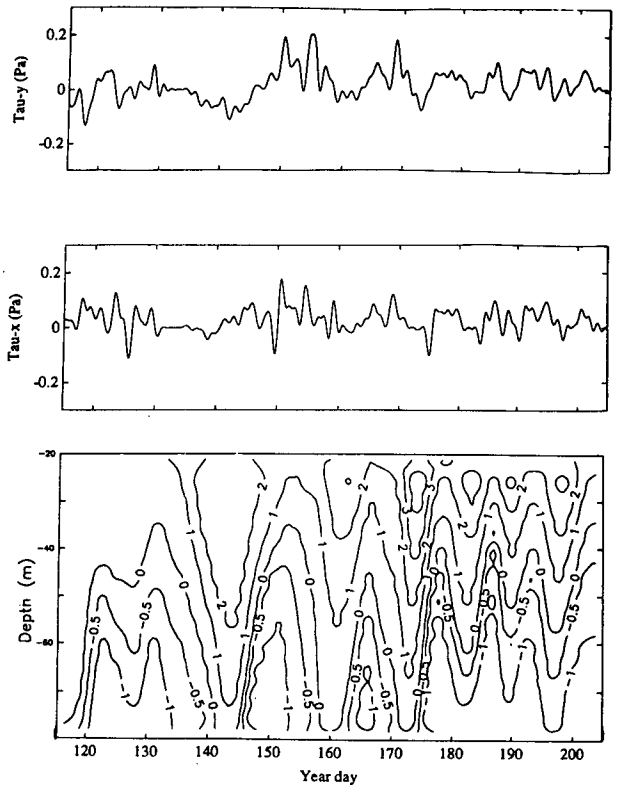

FIG. 6. Temperature (in °C) vs depth (in meters) and time (in days) at mooring 4 in 1990. St. John's wind stress (in Pa) for the same period is also shown. The wind stress is shown in component form using bay coordinates (see Fig. 2).

desired temperature is reached. This process is repeated for each time throughout the year. The method has its weaknesses in that the isotherm may be located above or below the vertical range of the thermistor chain and, also, the deepest depth with the desired temperature will always be chosen. Figure 7 shows the depth of the 1°C isotherm at moorings 2, 4, 5, and 6. (Note that a thermistor chain was not deployed at H1 and the thermistor chain at H3 failed.) The 1°C isotherm is chosen because it left the vertical range of the thermistor chain less often than any other value; however, the 2° or 0°C isotherms could have been used since the motion of these isotherms are very similar, as is apparent in Fig. 6. Figure 7 exhibits behavior similar to Figs. 5 and 6. Thermocline movement before ~ day 170 is better resolved in Fig. 7 than in Fig. 5 because using temperature at a fixed depth makes use of the vertical temperature stratification. As in Figs. 5 and 6, the motion of the thermocline appears to be driven by the along-bay wind stress.

A close examination of Fig. 7 reveals a number of interesting features of thermocline response in Conception Bay. First, the periods of the oscillations vary from 2 to 10 days, with the lower frequencies obviously more energetic. The higher frequencies also appear to have shorter length scales of coherence—for example, note the period from day 150 to 160. Second, displacements at H2 and H4 are roughly comparable in magnitude, as are those at H5 and H6, although there is a noticeable decrease in amplitude from the first to the second set. The head of the bay separates these two groups, so it may be that energy is lost as the Kelvin wave propagates around the head of the bay. Interaction with the topography inside of stations H5 and H6, which consists of three islands and a shallow shelf (<50 m), could also be important in scattering energy. Alternatively, the amplitude of the trapped wave response may be reduced because the moorings are effectively farther from the shoreline (see Fig. 2).

The data presented in this section show that there is a large response in the bay to wind events. Vertical displacements of tens of meters occur in response to the wind and are observed all around the head of the bay. Phase lag analysis of these data (not presented) show that propagation around the head of the bay is with a mean phase speed of ~ 0.7 m s^{-1}. This analysis shows that there is a propagating wave signal present in the data. In the next section we will develop a reduced-gravity model to apply to this system.

3. Model

To model the movements of the thermocline noted in the previous section and, in particular, to relate them more closely to the wind forcing, we take the simplest possible approach and drive a single-layer, reduced-gravity model with wind stress calculated from winds observed at St. John's airport. The governing equations are

$$\frac{\partial u}{\partial t} - fv = -g' \frac{\partial \eta}{\partial x} + \frac{\tau^x}{\rho_1 H} - \epsilon u, \tag{3.1}$$

$$\frac{\partial v}{\partial t} + fu = -g' \frac{\partial \eta}{\partial y} + \frac{\tau^y}{\rho_1 H} - \epsilon v, \tag{3.2}$$

$$\frac{\partial \eta}{\partial t} + H\left(\frac{\partial u}{\partial x} + \frac{\partial v}{\partial y}\right) = -\gamma \eta, \tag{3.3}$$

where u and v are velocity components in the x and y directions (see Fig. 2); f is the Coriolis parameter; ϵ and γ are Rayleigh friction and Newtonian damping parameters, respectively; and (τ^x, τ^y) is the surface wind stress. At 48°N, the latitude of Conception Bay, $f = 1.0 \times 10^{-4}$ s^{-1}. To interpret the model results, we shall imagine the pycnocline to be modeled by two layers of different density with the lower layer infinitely deep and at rest. In this approach, H is the undisturbed depth of the upper layer, η is the downward displacement of the interface between the layers, and g' is the reduced gravity given by $g' = g(\rho_2 - \rho_1)/\rho_1$, where g is the acceleration due to gravity, ρ_1 is the density of the upper layer, and ρ_2 the density of the lower layer.

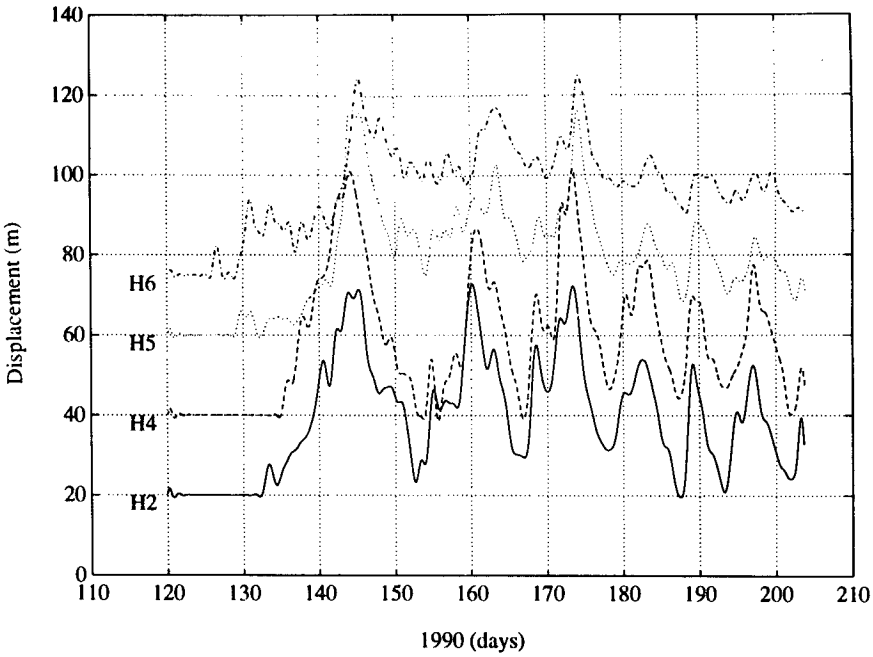

FIG. 7. Depth of the 1°C isotherm (in meters) at moorings H2, H4, H5, and H6. For easier comparison, 20 m has been added to the isotherm depth at H4, 40 m has been added to the isotherm depth at H5, and 60 m has been added to the isotherm depth at H6.

The applicability of this model to Conception Bay was discussed in the Introduction. In particular, the important parameter is

$$S = \frac{N_0^2 H_0^2}{f^2 L^2},$$

where N_0 and L are scales for the buoyancy frequency and the cross-shore topography in the bay and H_0 is the maximum depth (Wang and Mooers 1976; Huthnance 1978). The most representative way to estimate $N_0 H_0$ is to calculate vertical normal modes (as in Gill 1982) from the measured density field, assuming a bay of uniform depth equal to the maximum depth of the bay. If N is uniform in the vertical, then the corresponding wave speed for the first baroclinic normal mode is $c_1 = NH_0/\pi$ from which it follows that $S = c_1\pi/fL$. We have calculated c_1 for the two profiles shown in Fig. 4 (one is for 26 May 1990 and the other is for 22 June 1990) and obtained values of 0.53 and 0.59 m s^{-1}, respectively. Taking $L = 5$ km (see Fig. 1) then gives $S \sim 14$, indicating that coastal-trapped waves are likely to be strongly influenced by the density stratification, with characteristics similar to baroclinic, coastal Kelvin waves. We therefore feel that the use of the reduced-gravity model is justified.

The most important parameter in the above equations is the wave speed $c = \sqrt{g'H}$. At the end of the last section it was noted that phase lag analysis applied to the data shows that there is propagation around the head of the bay with a mean phase speed of ~0.7 m s^{-1}. This speed is similar to, though somewhat greater than, the wave speed calculated for the baroclinic first mode. As Clarke (1977) suggests, the observed propagation speed should be greater near the head of a bay because the radius of curvature of the coastline becomes comparable to the Rossby radius of deformation (in our case ~6 km). Thus, we should expect the observed speed from the Conception Bay array to be somewhat greater than that observed for a straight coastline. In practice, a range of values of g' and H have been used with the model. The best agreement with observations (over the period from day 150 to day 203 for 1990) being for values of $g' = 7.2 \times 10^{-3}$ m s^{-1} and $H = 40$ m, corresponding to a wave speed of 0.53 m s^{-1}. For the 1989 data we choose $g' = 9.6 \times 10^{-3}$ m s^{-1} and $H = 40$ m, corresponding to a wave speed of 0.62 m s^{-1}. These are the values adopted for g' and H in the model runs described in the next section.

We solve (3.1), (3.2), and (3.3) using the numerical method described by Heaps (1971). The method uses the Arakawa C-grid arrangement of u, v, and η with forward time differencing applied to (3.3) and backward time differencing to (3.1) and (3.2), with the exception of the Coriolis term in (3.2), which is treated using forward time differencing. There is no staggering in time, with each of u, v, and η being known at the same time and the new values of η, u, and v being obtained in that order.

The model results to be presented use a grid resolution of 1 km in each direction. This means that the

Rossby radius of deformation $c/f \sim 6$ km is well resolved by our grid and that Kelvin waves are well represented (Hsieh et al. 1983). Indeed, we have checked both the propagation speed of Kelvin waves and the maximum group velocity of Poincaré waves and found both to be equal to the analytical value.

Figure 8 shows the two model domains used. The first contains only Conception Bay while the second includes Trinity Bay as well. Comparison between the results for each domain will be used to assess the importance of wind forcing over Trinity Bay. The boundary formulation used on the open ocean parts of the model domain is discussed in detail in Greatbatch and Otterson (1991). The positioning of the open ocean part of the western boundary (the "upstream" boundary in the sense of Kelvin wave propagation) is the most important feature of this boundary formulation. It should be noted that it does not meet the coastline at an angle; rather, it is a continuation of the coast. In this way, coastal up/downwelling calculated by the model will be due solely to Ekman divergence/convergence along the coastline within the model domain, with no inference being made about regions outside the model domain. On the northern and eastern boundaries, an Orlanski (1976) radiation condition is applied to η but using forward-in-time upstream differencing as suggested by Miller and Thorpe (1981). The use of the C-grid means that one of the components of velocity (actually that parallel to the boundary) must also be set on the boundary. We do this by requiring the normal derivative of this velocity component to be zero on the boundary. On the open ocean part of the western boundary, the radiation condition on η is replaced by one of no normal derivative (Greatbatch and Otterson 1991).

It was noted in section 2 that the wind stress used to drive the model is assumed to be spatially uniform and is derived from winds measured at St. John's airport. As noted in section 2, all the data discussed in this paper have been low-pass filtered in order to remove energy with period less than 32 h. This is also true of the wind stress used to drive the model. The wind stress was calculated from unfiltered wind and the resulting wind-stress time series filtered. This low-pass filtering of the wind means that all propagating inertia–gravity (Poincaré) waves that form part of our

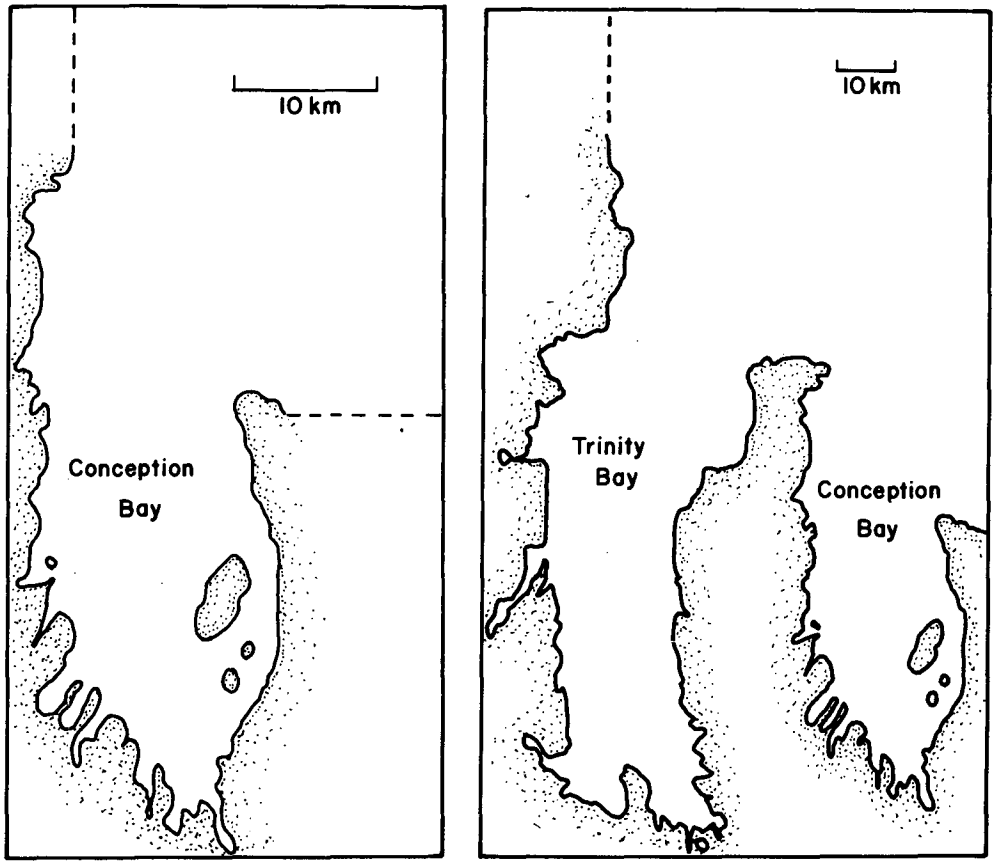

FIG. 8. The two model domains used to simulate Conception Bay: (a) local and (b) nonlocal. An artificial stretch of straight coastline has been added to the east of Cape St. Francis. The dashed line section in the northwestern part of each domain represents the position of the boundary condition $\eta_x = 0$.

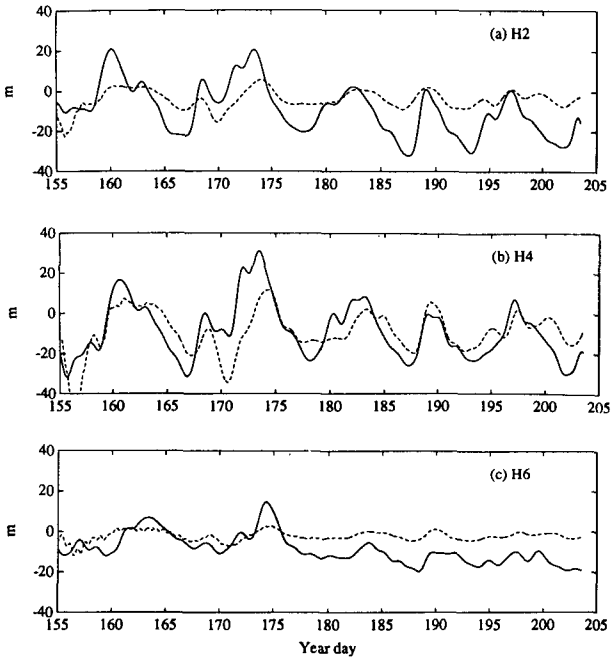

FIG. 9. Interface displacement at moorings (a) H2, (b) H4, and (c) H6. The solid line shows the observed displacement of the 1°C isotherm, the dashed line the model results. Model results were obtained from the local model (Fig. 8a).

model solution must be generated at the initial startup. In fact, all the model runs to be described are initialized with $u = v = \eta = 0$. The wind stress is suddenly turned on at the start of the integration, thus generating an entire spectrum of transients. Some of these propagate quickly out of the model domain, but a weak damping ($\gamma = \epsilon = 1/10$ days) is necessary to remove near-inertial Poincaré waves that otherwise would persist. We have investigated the sensitivity of our model to startup time (i.e., the day at which the model run begins) and have found no sensitivity once the initial transients have died away ($\sim$10 days into the integration).

4. Comparisons of model results with observations

In this section, we present model results for the two different model domains and then compare the results. First, we look at the local domain (Fig. 8a), which treats only Conception Bay, and then add Trinity Bay to the model (Fig. 8b) to include nonlocal effects. The parameters used in the model runs are discussed in the previous section.

a. Local model

In this section we use the model domain shown in Fig. 8a, using just Conception Bay, the local model. Figure 9 compares model-calculated interface displacement with the depth of the 1°C isotherm at moorings 2, 4, and 6. The model interface displacement, η, corresponds to downward displacement and compares well with the movement of the 1°C isotherm, also measured positive downward. There is a strong correlation between the model and the observations, although the model generally underpredicts the amplitude of the response and also does not always produce a good match in phase. Correlation coefficients between the model and observations vary between 0.50 at zero lag (H6) and 0.58 with a lead of $\sim$0.25 days (H2) (see Table 1). (Lag means that the model lags the data and lead means that the model is ahead of the data.) Phase matching in the local model is not strongly sensitive to the choice of parameters because a Kelvin wave propagates around the coastline within the model domain in a little over a day, a short time compared to the dominant period of oscillation in the observations. The amplitude can be varied by adjusting H, keeping $g'H$ constant, because of the dependence of the wind forcing term on $1/H$ in (3.1) and (3.2). As we shall see, however, the amplitude discrepancy is greatly reduced once the effect of Trinity Bay is included.

Figure 10 shows the principal component of velocity observed at depth $\sim$25 m and modeled velocities at moorings H1, H3, H4, and H6. The data were analyzed to find the principal components from the various current records, since for Kelvin waves we expect the alongshore velocity to dominate. For moorings H1 and H3, the cross-shore component in the model and observations is nearly zero. In all cases the alongshore component of velocity was much larger than the cross-shore component, as expected within the coastal waveguide close to the shore. The velocity component extracted from the model is aligned with the mooring data at each location; hence, the direction of the alongshore velocity changes from mooring to mooring (by a few tens of degrees) in the same way for the model data and the measured observations. The model and observed alongshore velocities (Fig. 10) show some agreement at H1; good agreement at H3, which is the closest of all of the stations to the shoreline; and relatively poor agreement at H4 and H6. At H3, where the agreement is best, the model overpredicts the amplitude of the current, which is interesting since it underpredicts

TABLE 1. Correlations (K) and phase lags (Φ) between the model and data isotherm displacements for mooring stations H2, H4, H5, and H6. A positive lag indicates that the model leads the data and a negative lag that the data leads the model.

	Local		Nonlocal	
	K	Φ (days)	K	Φ (days)
H1	0.58	+0.25	0.75	1.0
H2	0.55	+1.0	0.75	−1.0
H5	0.52	0	0.75	2.0
H6	0.50	0	0.55	1.5

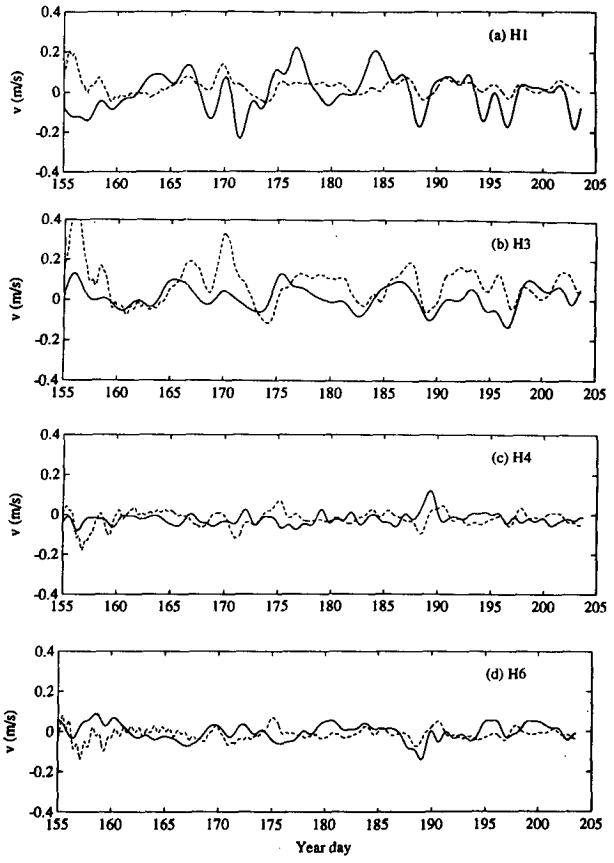

FIG. 10. Alongshore component of velocity at 25-m depth computed from principal component analysis of the mooring data for (a) H1, (b) H3, (c) H4, and (d) H6. The solid line shows the observations, the dashed line the model results. Model results were obtained using the local model (Fig. 8a).

the thermocline response at the nearby location H2 (Fig. 9).

In summary, the local model does reasonably well in simulating the isotherm deflections, certainly well enough to show that the simple wind-forced model explains much of the up/downwelling in the bay. The model does poorly in simulating the observed currents at 25-m depth. This failure is in some ways not surprising given the simplicity of the vertical structure of the model. For example, in the model the surface Ekman component of the flow is combined with the pressure-driven response (Gill 1982) into a single velocity, whereas in reality we expect the Ekman component to be confined near the surface with the pressure-driven part distributed over the depth of the water column. We show in the next section that the nonlocal model does much better, both in simulating the current and the thermocline response.

b. Nonlocal model

The parameters used in the nonlocal model are the same as those used in the previous section for the local model; only the model domain has been changed. Here we consider the effect of adding Trinity Bay to the domain (see Fig. 1 for the area map and Fig. 8b for the model domain). As discussed in section 3, the upstream boundary conditions for the nonlocal model are set in the same way as those for the local one. In particular, at the upstream end no incoming energy is permitted and at the eastern boundary all of the energy is allowed to leave the model domain.

Figure 11 shows the comparison between the model-calculated interface displacement and the observations at the same stations as discussed for the local model: H2, H4, and H6. The results at H2 in particular show a significant improvement as compared to the local model (Fig. 9). Both amplitude and phase now agree quite well. Correlation coefficients between the model and observations vary from 0.55 at H6 to 0.70–0.75 at H2, H4, and H5. The correlation coefficients and lags for the local and nonlocal model are shown in Table 1. At some locations the model leads the data (as opposed to the lag found in the local model) by as much as 1–2 days (e.g., H5 and H6). For all stations, the nonlocal model shows an improvement over the local model (see Table 1) though not always at zero lag. The tendency of the model to underpredict the amplitude has been eliminated and there is strong correlation between the model results and the observations. At H6, it appears that the nonlocal model does somewhat better than the local model (Fig. 9), though

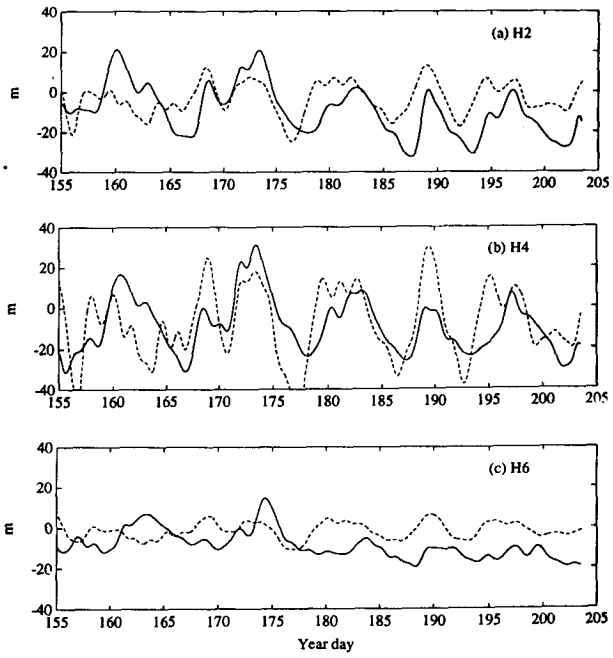

FIG. 11. Interface displacements at moorings (a) H2, (b) H4, and (c) H6. The solid line shows the observed displacement of the 1° isotherm, the dashed line the model results. Model results were obtained using the nonlocal model (Fig. 8b).

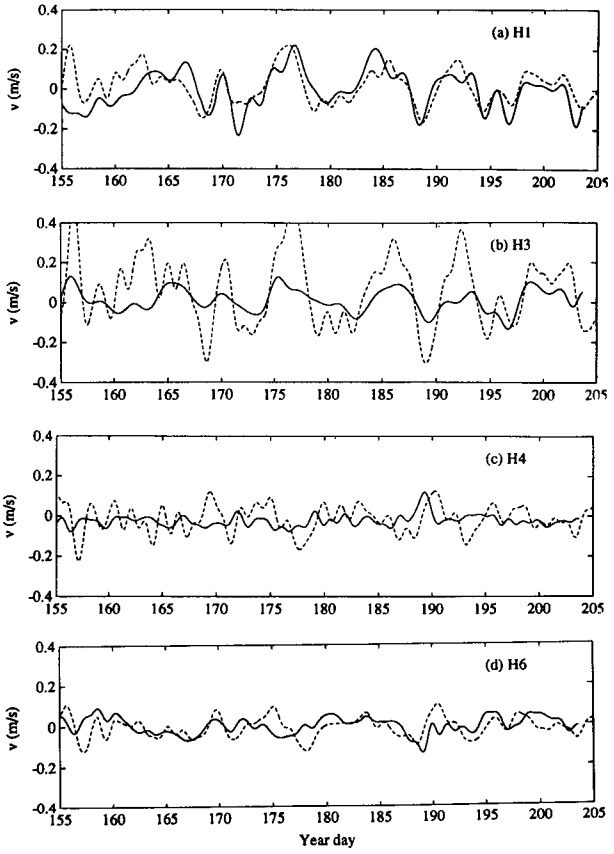

FIG. 12. Alongshore component of current at 25-m depth from moorings (a) H1, (b) H3, (c) H4, and (d) H6. The solid line shows the observations, the dashed line the model results. Model results were obtained using the nonlocal model (Fig. 8b).

not by much. The local model underpredicts the amplitude (Fig. 9c) while the nonlocal model does not match the phase well, though the amplitude is reasonably well simulated in the nonlocal model, at least for times beyond day 170. These conclusions are supported by correlation analysis, which shows a 1.5-day lag at H6 for the nonlocal model versus zero lag for the local model. Thus, the nonlocal model does marginally better overall beyond the head of the bay. These results do show that the nonlocal model does better up to the head of Conception Bay but do not prove the influence of Trinity Bay beyond the head of Conception Bay.

Comparison between modeled and observed currents shows even more improvement in using the nonlocal model versus the local one. Figure 12 shows the currents at H1, H3, H4, and H6. In all cases, except at H4 located at the head of the bay, there is a correlation in the alongshore current between model and data. The results from the local model show at best only a very weak correlation with the observations. Thus, even though we might not expect good correlation using a reduced-gravity model, we in fact find quite strong correlations with the observed surface currents as measured at a fixed depth. At H6 it appears that the nonlocal model (Fig. 12d) does somewhat better at simulating the currents than the local model (Fig. 10d), just as we found for the displacement. The signal in both displacement and current at H6 is weak, however, and it is not clear from this analysis how important the influence of Trinity Bay is beyond the head of Conception Bay. At the one station closest to shore, H3, we find that the agreement with the nonlocal model is actually worse than that for the local model. This discrepancy may be due to the enhanced movement of the thermocline at that location and hence aliasing of the current signal as measured by the current meters. The difference may also indicate the local influence of bottom topography at this particular station, which is less than 1 km away from the coast.

The influence of Trinity Bay can be determined by differencing the results of the two models. The amplitude of this difference reaches 20 m near the head of the bay and is comparable in amplitude to the wind-forced signal itself. It might be expected that the importance of Trinity Bay would be more apparent the farther north one moves along the western side of Conception Bay and indeed this is true. Figure 13a compares the interface displacement as calculated by the local model with the observed thermocline response for 1989, using data from M1 and the model parameters as discussed in section 3. The only difference in the parameters is that $\Delta\rho = 1.0$ for the 1989 runs compared to $\Delta\rho = 0.7$ for the 1990 runs. The local model fails to represent the observed response though there are a few signs of some correlation. The model underpredicts the amplitude by about an order of magnitude, and does not reproduce the major events. Figure 13b, on the other hand, shows a comparison between the nonlocal model and the observed response at M1. The nonlocal model, including Trinity Bay, does much better, estimating the amplitude fairly closely and also simulating most of the major events. These comparisons show that near the mouth on the western side of Conception Bay, Trinity Bay exerts much more influence than does purely local forcing.

These observations near the mouth of Conception Bay further confirm the importance of Trinity Bay and are in line with the nature of a wind-driven upwelling response, which is expected to be a maximum at the end of an alongshore unidirectional section of coast. Thus, near the mouth at M1, Trinity Bay dominates, while near the head of the bay, H1–H6, the nonlocal and local response are about equally important. Beyond the head of the bay, at H5–H6, the influence of Trinity Bay is less noticeable. Indeed, in this region the local model performs just as well as, or perhaps better than, the nonlocal model. This may well be due to scattering of coastal-trapped waves by the shallow bottom topography in this region (see Fig. 1).

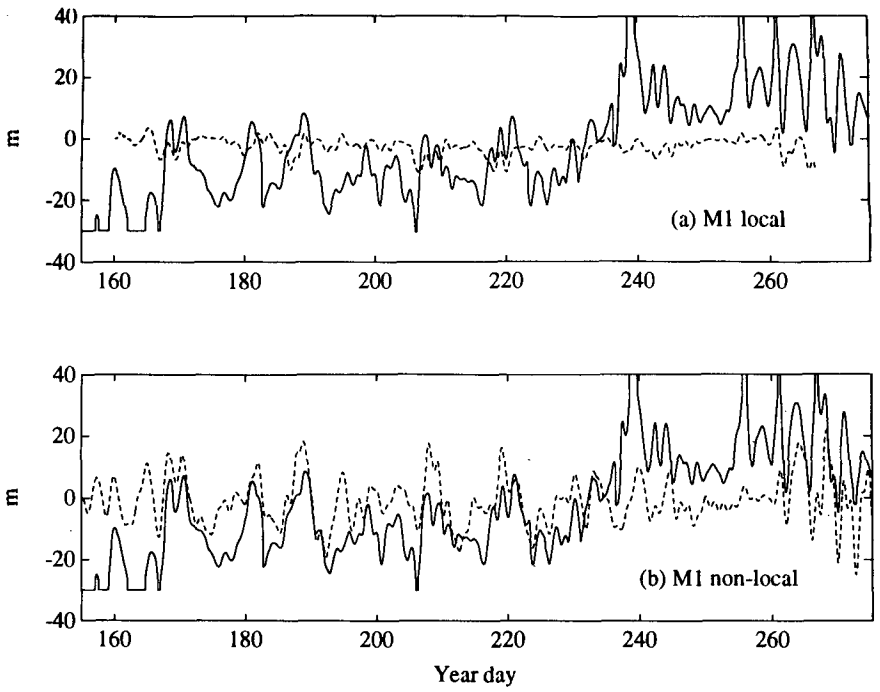

FIG. 13. Interface displacement at M1 (Fig. 1) as determined from (a) the local and (b) the nonlocal model (dashed line) and the observed displacement of the 1° isotherm (solid line).

5. Summary and discussion

We have used data from Conception Bay, Newfoundland, to investigate the importance of wind forcing over the bay. The dominant signal in the temperature and surface current records is at periods of 2–10 days and appears to be associated with the local wind. This is most obvious for the temperature data, which is strongly correlated with the local wind. Analysis of temperature data, collected in 1990 around the head of the bay, shows that the signal is coherent around the head of the bay from the western to the eastern side. There is some diminution in the amplitude of the response on the eastern side suggesting that the wave is either scattered or dissipated as it propagates around the head. We have noted that the water is much shallower on the southeast side of the bay, near Bell Island, and it is possible that coastal-trapped waves are scattered in this region (Killworth 1989a,b). Surface current data do not appear to be strongly correlated with the local wind, exhibiting more complicated behavior than the temperature data.

We developed a simple, reduced-gravity model forced by the local wind in an effort to understand the relationship between the wind forcing and the internal response. Such a model ignores the influence of bottom topography but does include all of the detail of the coastal geometry. We have argued that the model is applicable to Conception Bay. This is because the sides of the Bay are very steep, so that although the density stratification is relatively weak compared to more tropical latitudes, the stratification parameter

$$S = \frac{N_0^2 H^2}{f^2 L^2}$$

has a value ~10 (Wang and Mooers 1976; Huthnance 1978). We applied two versions of this model, one that included a neighboring bay (the nonlocal model) and a second that included only Conception Bay (the local model). By using the boundary formulation of Greatbatch and Otterson (1991), we have ensured that any coastal up/downwelling calculated by the model is due only to the Ekman divergence/convergence from the coastline within the model domain. In particular, no inferences are made about the nature of the coastline and wind-stress field beyond the model domain. The local model did reasonably well near the head of the bay though the currents at 25-m depth were poorly simulated and the amplitude of the thermocline displacement was underpredicted. On the western side of the bay near the mouth, the local model simulated neither the measured currents nor the thermocline displacement. The nonlocal model, on the other hand, was quite successful near the mouth and near the head of the bay in simulating both the interface displacement and the measured current. Beyond the head of the bay, the local model did nearly as well as the nonlocal model. The difference between the results of the two models shows the importance of nonlocal forcing.

The success of the model developed here shows that even simple models can provide realistic simulations when applied to a bay. It is remarkable how well the model does in simulating both the thermocline displacement and the measured current. These results have direct application to the wind-forced studies of Leggett et al. (1984) mentioned in the Introduction. Any attempt to use the wind as an index of upwelling in a local system, such as Conception Bay, must take into account the nonlocal forced response that propagates into the system, particularly on the western side of the bay. On the western side of the bay, near the mouth, the nonlocal response dominates.

Although this model does quite well at reproducing the observations, there are clearly things that can be done using a more sophisticated model. In particular the influence of bottom topography should be considered in detail. It is probably best to develop a 3D primitive equation model to allow for isopycnals to intersect the bottom topography [Killworth (1989b) has shown that this is important for the scattering of coastal-trapped waves]. This will also allow us to compare model output with the current meter data in more detail and also at different depths. Determination of the structure of the propagating waves, whether they are fully baroclinic Kelvin waves, barotropic shelf waves, or some hybrid (Huthnance 1978), will require a different mooring array to provide information about the vertical and cross-slope structure. Both winter and summer data would be needed to determine the influence of changing stratification upon the nature of the response. It would also be useful to reanalyze the data presented by Yao (1986) to look more closely at the question of propagation of coastal-trapped waves around Trinity Bay.

Acknowledgments. This work has been funded by the Natural Sciences and Engineering Research Council (NSERC) through a strategic grant, the Cold Ocean Productivity Experiment (COPE). We are grateful to J. Foley and K. Forward for assistance with the field work and with processing of the current meter and CTD data. Comments from two reviewers helped improve the manuscript.

REFERENCES

Clarke, A. J., 1977: Observational and numerical evidence for wind-forced coastal trapped long waves. *J. Phys. Oceanogr.*, **7**, 231–247.

deYoung, B., and B. Sanderson, 1992: Seasonal cycles and mean circulation in Conception Bay, Newfoundland. *Atmos.-Ocean*, submitted.

Farmer, D. M., and T. R. Osborn, 1976: The influence of the wind on the surface layer of a stratified inlet. Part 1: Observations. *J. Phys. Oceanogr.*, **6**, 931–940.

Frank, K. T., and W. C. Leggett, 1981: Wind regulation of emergence times and early survival in capelin (*Mallotus villosus*). *Can. J. Fish. Aquat. Sci.*, **38**, 215–223.

——, and ——, 1982: Coastal water mass replacement: Its effect on zoo-plankton and the predator–prey complex associated with larval capelin (*Mallotus villosus*). *Can. J. Fish. Aquat. Sci.*, **39**, 991–1003.

Gill, A. E., 1982: *Atmosphere–Ocean Dynamics.* Academic Press, 662 pp.

——, and A. J. Clarke, 1974: Wind-induced upwelling, coastal currents, and sea-level changes. *Deep-Sea Res.*, **21**, 325–345.

Greatbatch, R. J., and T. Otterson, 1991: On the formulation of open boundary conditions at the mouth of a bay. *J. Geophys. Res.*, **96**, 18 431–18 445.

Heaps, N. S., 1971: On the numerical solution of the three-dimensional hydrodynamical equations for tides and storm surges. *Mem. Soc. R. Sci. Liege*, Ser. 6, 143–180.

Hsieh, W. W., M. K. Davey, and R. C. Wajsowicz, 1983: The free Kelvin wave in finite-difference numerical models. *J. Phys. Oceanogr.*, **13**, 1383–1397.

Huthnance, J. M., 1978: On coastal trapped waves: Analysis and numerical calculation by inverse iteration. *J. Phys. Oceanogr.*, **8**, 74–92.

Johnson, M. A., and J. J. O'Brien, 1990a: The northeast Pacific Ocean response to the 1982–1983 El Niño. *J. Geophys. Res.*, **95**(C5), 7155–7166.

——, and ——, 1990b: The role of coastal Kelvin waves on the northeast Pacific Ocean. *J. Mar. Syst.*, **1**, 29–38.

Killworth, P. D., 1978: Coastal upwelling and Kelvin waves with small longshore topography. *J. Phys. Oceanogr.*, **8**, 188–205.

——, 1989a: How much of a baroclinic coastal Kelvin wave gets over a ridge? *J. Phys. Oceanogr.*, **19**, 321–341.

——, 1989b: Transmission of a two-layer coastal Kelvin wave over a ridge. *J. Phys. Oceanogr.*, **19**, 1131–1148.

Klinck, J. M., J. J. O'Brien, and H. Svendsen, 1981: A simple model of fjord and coastal circulation interaction. *J. Phys. Oceanogr.*, **11**, 1612–1626.

Large, W. G., and S. Pond, 1981: Open ocean momentum flux measurements in moderate to strong winds. *J. Phys. Oceanogr.*, **11**, 324–336.

Leggett, W. C., K. T. Frank, and J. E. Carscadden, 1984: Meteorological and hydrographic regulation of year-class strength in capelin (*Mallotus villosus*). *Can. J. Fish. Aquat. Sci.*, **41**, 1193–1201.

Miller, M. J., and A. J. Thorpe, 1981: Radiation conditions for the lateral boundaries of limited-area numerical models. *Quart. J. Roy. Meteor. Soc.*, **107**, 615–628.

Orlanski, I., 1976: A simple boundary condition for unbounded hyperbolic flows. *J. Comput. Phys.*, **21**, 251–269.

Pares-Sierra, A., and J. J. O'Brien, 1989: The seasonal and interannual variability of the California Current system: A numerical model. *J. Geophys. Res.*, **94**(C4), 3159–3180.

Petrie, B., and C. Anderson, 1983: Circulation on the Newfoundland continental shelf. *Atmos.-Ocean*, **21**, 207–226.

——, J. W. Loder, S. Akenhead, and J. Lazier, 1991: Temperature and salinity variability on the eastern Newfoundland shelf: The annual harmonic. *Atmos.-Ocean*, **29**, 14–36.

Proehl, J. A., and M. Rattray, Jr., 1984: Low-frequency response of wide deep estuaries to non-local atmospheric forcing. *J. Phys. Oceanogr.*, **14**, 904–921.

Smith, P. C., and J. I. MacPherson, 1987: Cross-shore variations of near-surface wind velocity and atmospheric turbulence at the land–sea boundary during CASP. *Atmos.-Ocean*, **25**, 279–303.

Svendsen, H., and R. O. R. Y. Thompson, 1978: Wind-driven circulation in a fjord. *J. Phys. Oceanogr.*, **8**, 703–712.

Taggart, C. T., and W. C. Leggett, 1987: Wind-forced hydrodynamics and their interaction with larval fish and plankton abundance: A time-series analysis of physical–biological data. *Can. J. Fish. Aquat. Sci.*, **44**, 438–451.

Wang, D.-P., 1979: Wind driven circulation in the Chesapeake Bay, winter 1975. *J. Phys. Oceanogr.*, **9**, 564–572.

——, and C. N. K. Mooers, 1976: Coastal-trapped waves in a continuously stratified ocean. *J. Phys. Oceanogr.*, **6**, 853–863.

Yao, T., 1986: The response of currents in Trinity Bay, Newfoundland, to local wind forcing. *Atmos.-Ocean*, **24**, 235–252.